

Supplementary Information

Building a stable cationic molecule/electrode interface for highly efficient and durable CO₂ reduction at an industrial-relevance current

Jianjun Su,^a Jun-Jie Zhang,^b Jiacheng Chen,^c Yun Song,^a Libei Huang,^a Minghui Zhu,^{*c} Boris I. Yakobson,^b Benzhong Tang,^{d,e,f} and Ruquan Ye^{*a,g}

^aDepartment of Chemistry, State Key Lab of Marine Pollution, City University of Hong Kong, Hong Kong 999077, China.

^bDepartment of Materials Science and Nano Engineering and Department of Chemistry, Rice University, 6100 Main Street, Houston, Texas 77005, USA.

^cState Key Laboratory of Chemical Engineering, East China University of Science and Technology, Shanghai 200237, China.

^dDepartment of Chemistry, Hong Kong Branch of Chinese National Engineering Research Center for Tissue Restoration and Reconstruction and Institute for Advanced Study, SCUT-HKUST Joint Research Institute, The Hong Kong University of Science and Technology, Clear Water Bay, Kowloon, Hong Kong 999077, China.

^eHKUST-Shenzhen Research Institute, No. 9 Yuexing 1st Rd, South Area, Hi-tech Park, Nanshan, Shenzhen 518057, China.

^fCenter for Aggregation-Induced Emission, State Key Laboratory of Luminescent Materials and Devices, South China University of Technology, Tianhe Qu, Guangzhou 510640, China

^gCity University of Hong Kong Shenzhen Research Institute, Shenzhen, Guangdong 518057, China.

Corresponding author. E-mail: minghuizhu@ecust.edu.cn, ruquanye@cityu.edu.hk

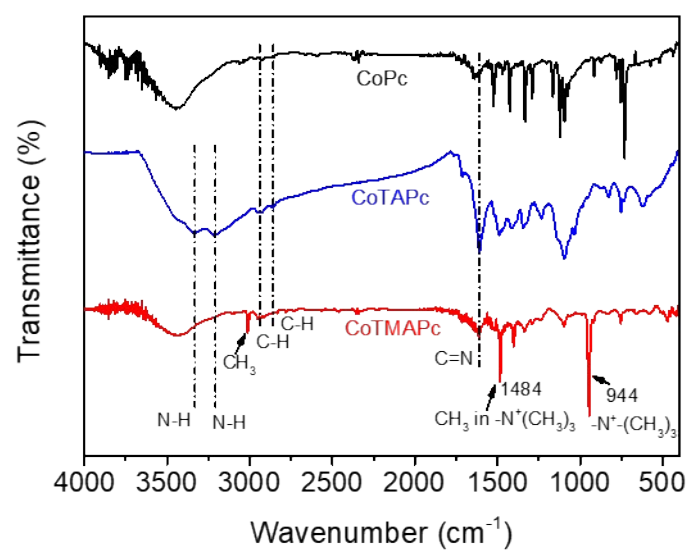


Fig. S1. FT-IR spectra of CoPc, CoTAPc and CoTMAPc.

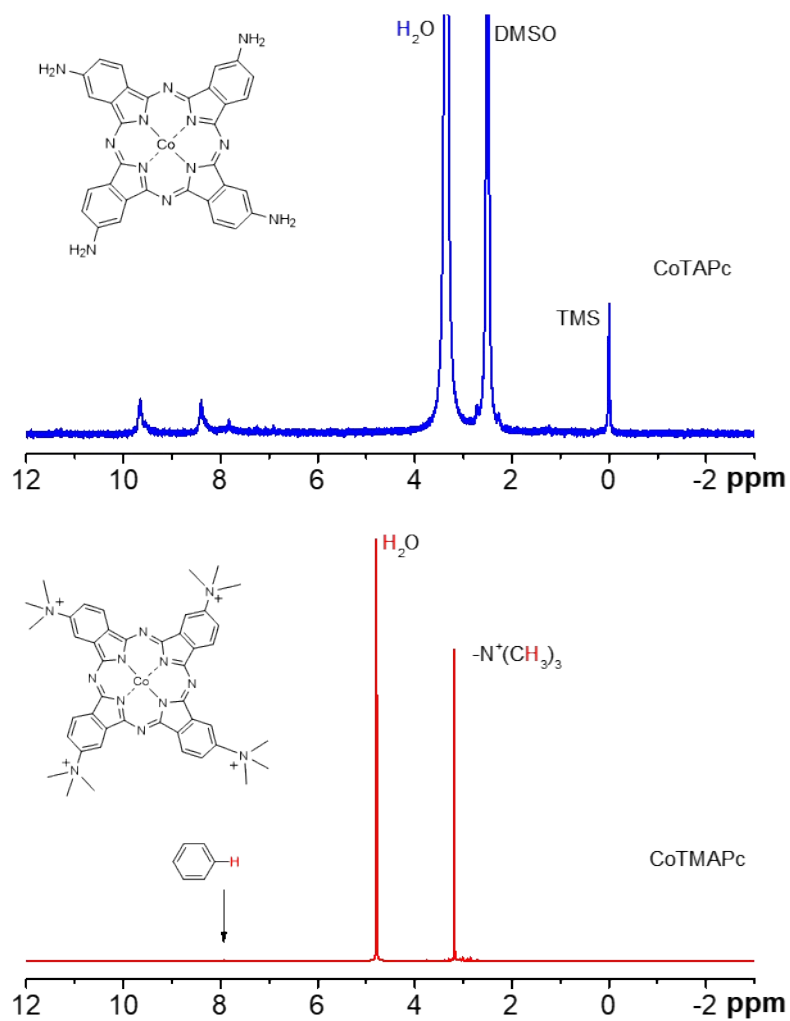


Fig. S2. ¹H NMR spectra of CoTAPc and CoTMAPc. ¹H NMR spectra of CoTAPc and CoTMAPc were measured in DMSO-d₆ and D₂O solvent, respectively.

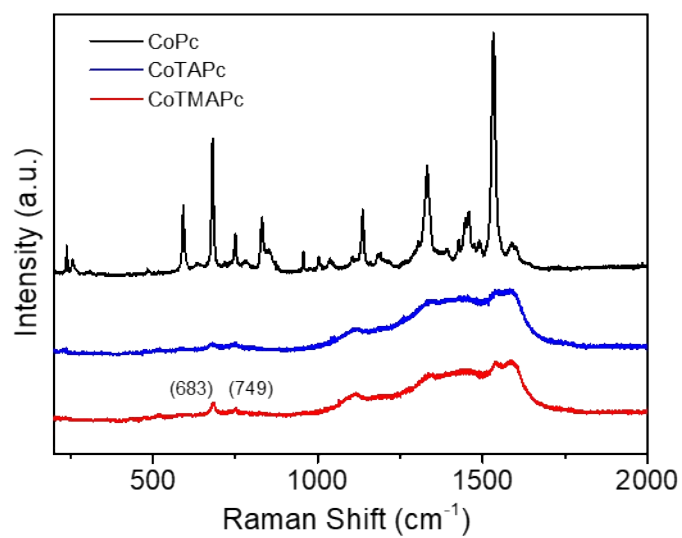


Fig. S3. Raman spectra of CoPc, CoTAPc and CoTMAPc.

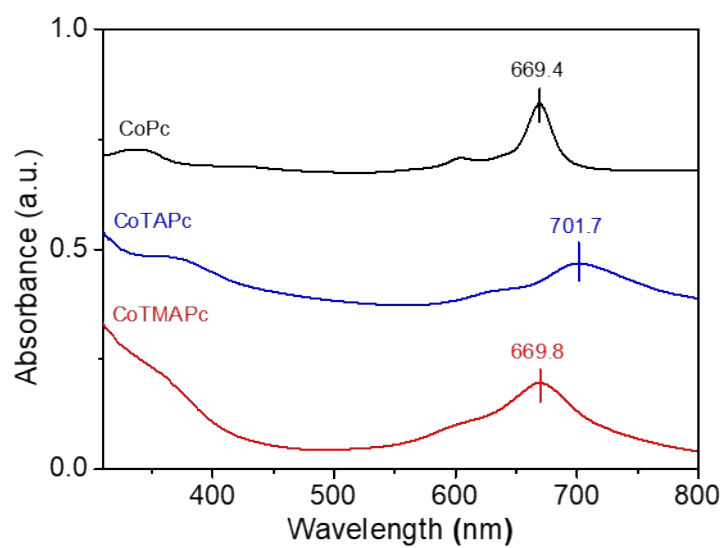


Fig. S4. UV-vis spectra of CoPc, CoTAPc and CoTMAPc in DMF.

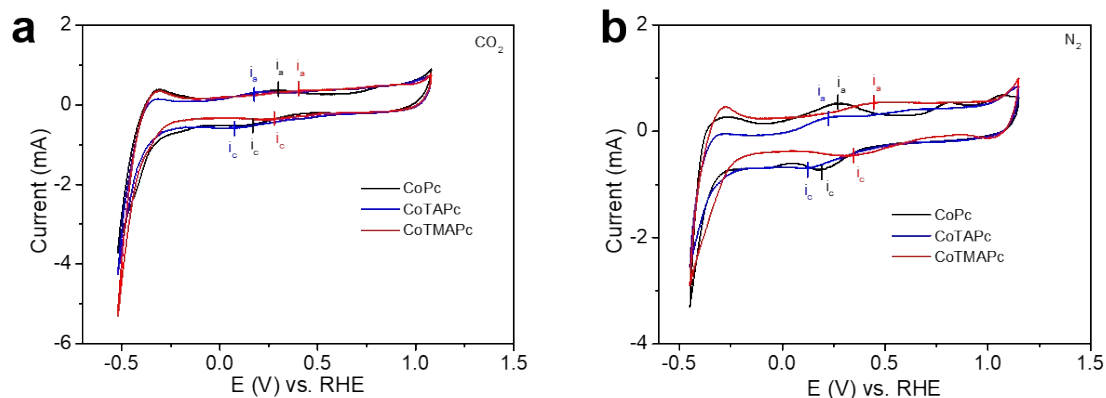


Fig. S5. CV curves of CoPc, CoTAPc and CoTMAPc under CO₂ (a) and N₂ (b) at a scan rate of 500 mV/s in 0.5 M aqueous KHCO₃. The anodic and cathodic peak are labelled as *i_a* and *i_c*.

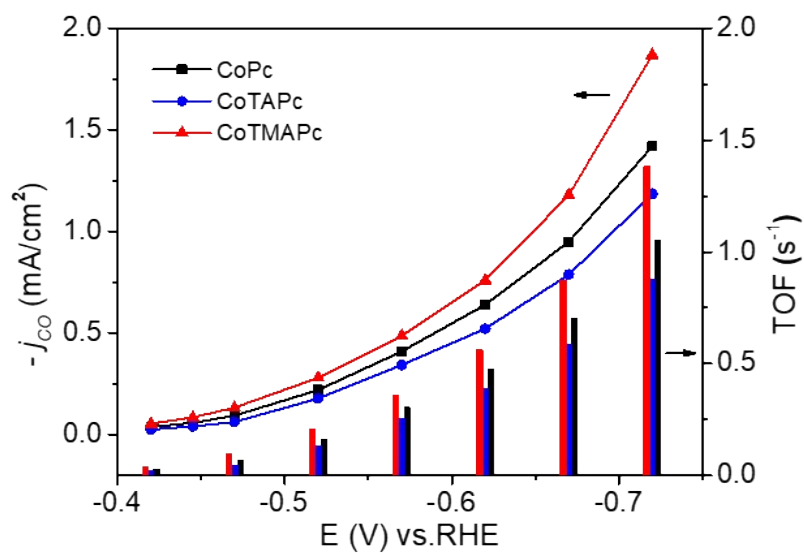


Fig. S6. CO partial current densities and TOF_{CO} values of CoPc, CoTAPc and CoTMAPc.

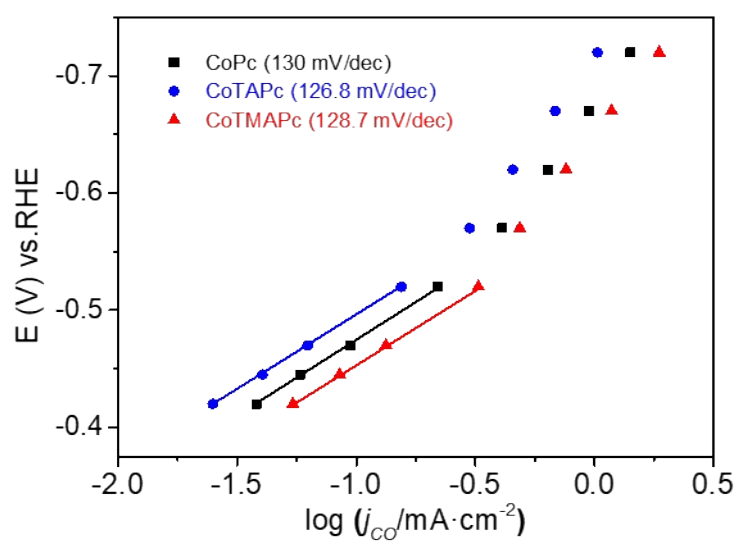


Fig. S7. Tafel plots of CoPc, CoTAPc and CoTMAPc, the catalyst loading is $7 \times 10^{-9} \text{ mol/cm}^2$.

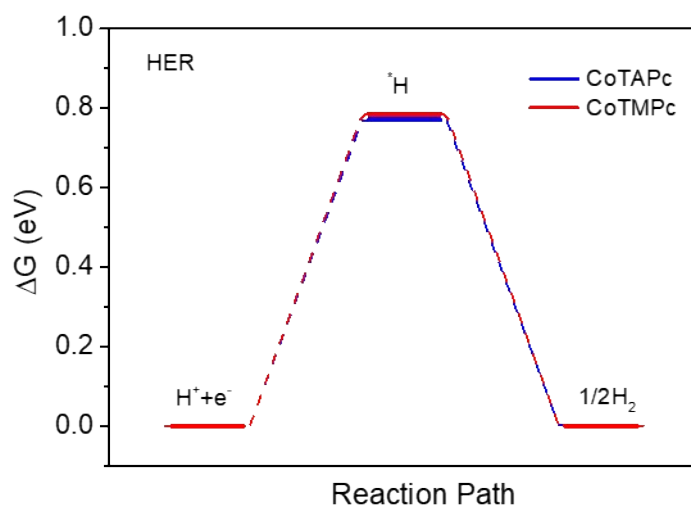


Fig. S8 Hydrogen evolution reaction (HER) free energy profiles of CoTAPc and CoTMAPc

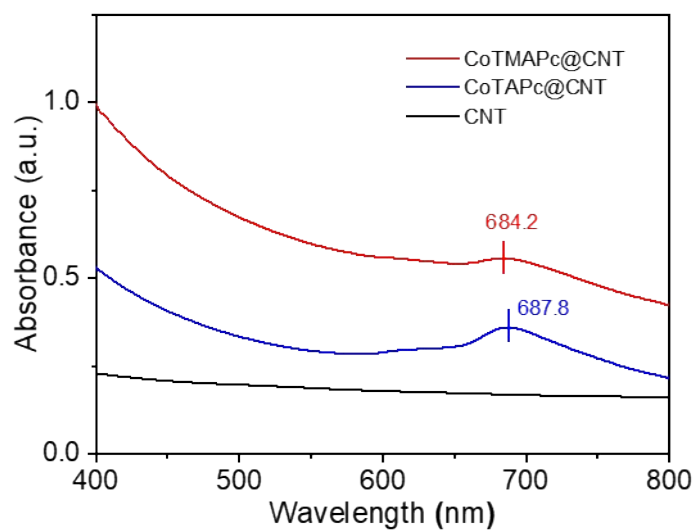


Fig. S9. UV-vis spectra of pristine CNT, CoTAPc@CNT and CoTMAPc@CNT in DMF.

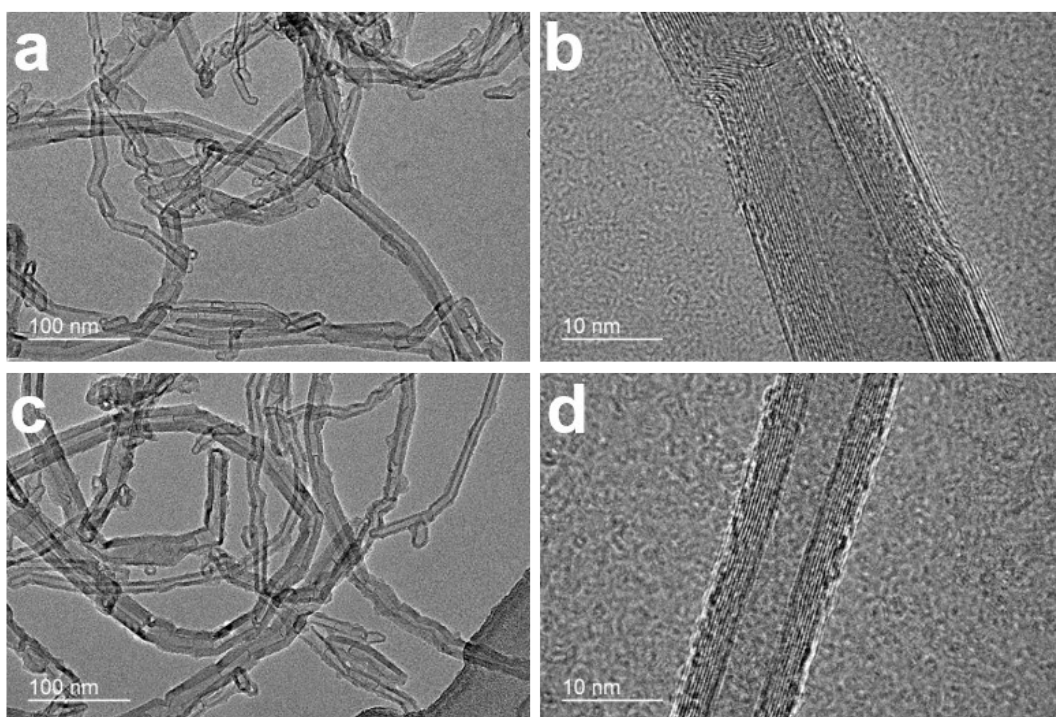


Fig. S10. TEM images of (a, b) pristine CNT, and (c, d) CoTAPc@CNT.

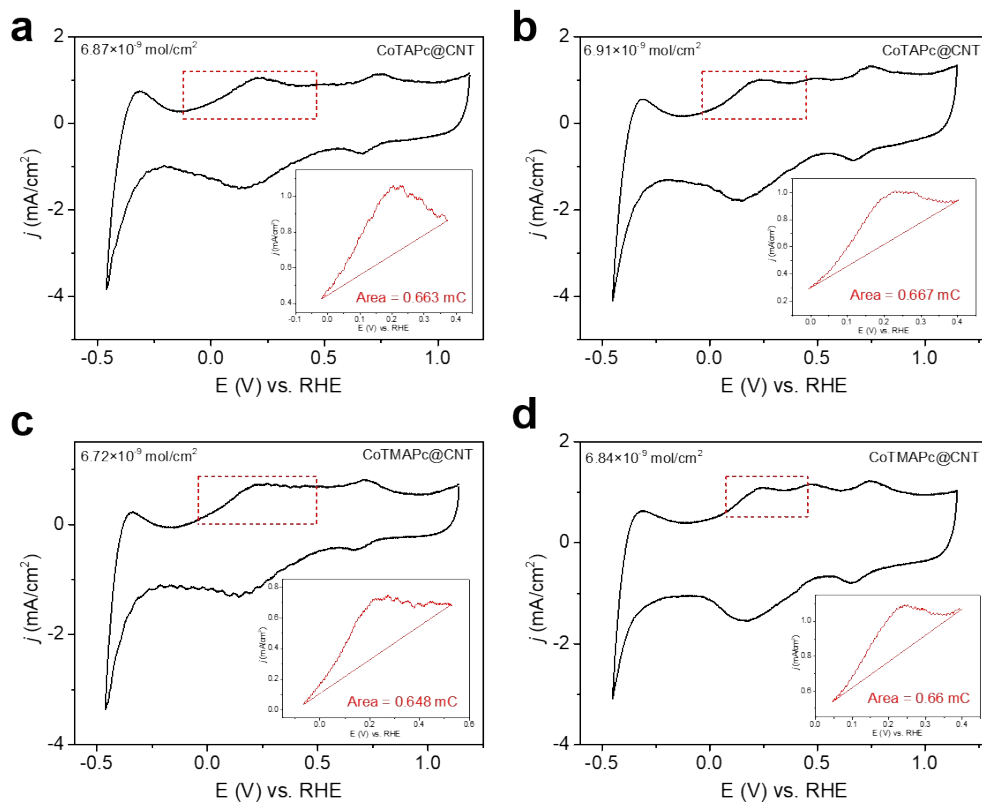


Fig. S11. CV curves of (a, b) before and after 30 min chronoamperometric test of CoTAPc@CNT and (c, d) before and after 30 min chronoamperometric test of CoTMAPc@CNT in N_2 saturated 0.5 M KHCO_3 (pH 8.36) at a rate of 0.5 V/s. Insert shows the enlarged region (anodic peak from the $\text{Co}^{\text{I}}/\text{Co}^{\text{II}}$). The surface active Co site is calculated as Method 1.

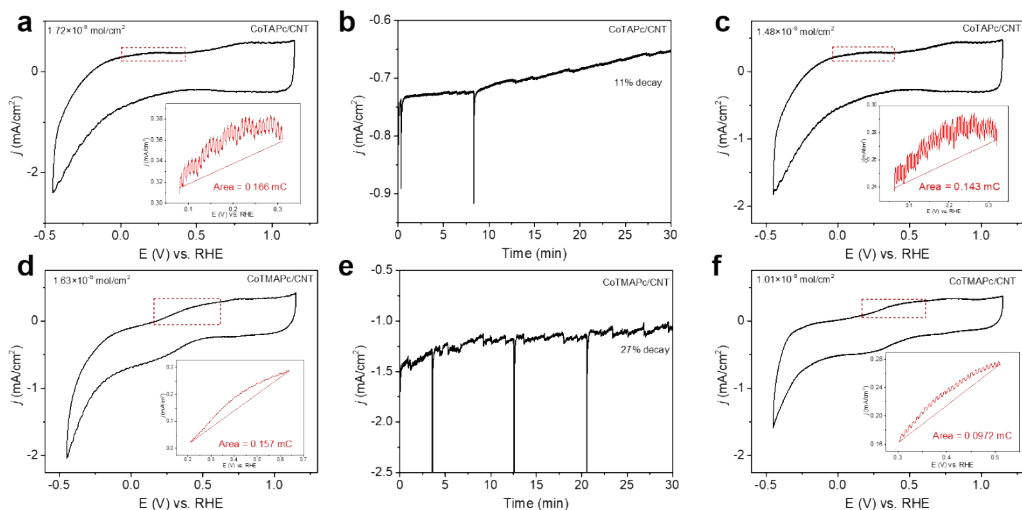


Fig. S12. CV curves of (a, c) before and after 30 min chronoamperometric test of CoTAPc/CNT and (d, f) before and after 30 min chronoamperometric test of CoTMAPc/CNT in N_2 saturated 0.5 M $KHCO_3$ (pH 8.36) at a rate of 0.5 V/s. Long-term electrolysis of (b) CoTAPc/CNT and (e) CoTMAPc/CNT were performed in CO_2 saturated 0.5 M $KHCO_3$ at -0.62 V versus RHE.

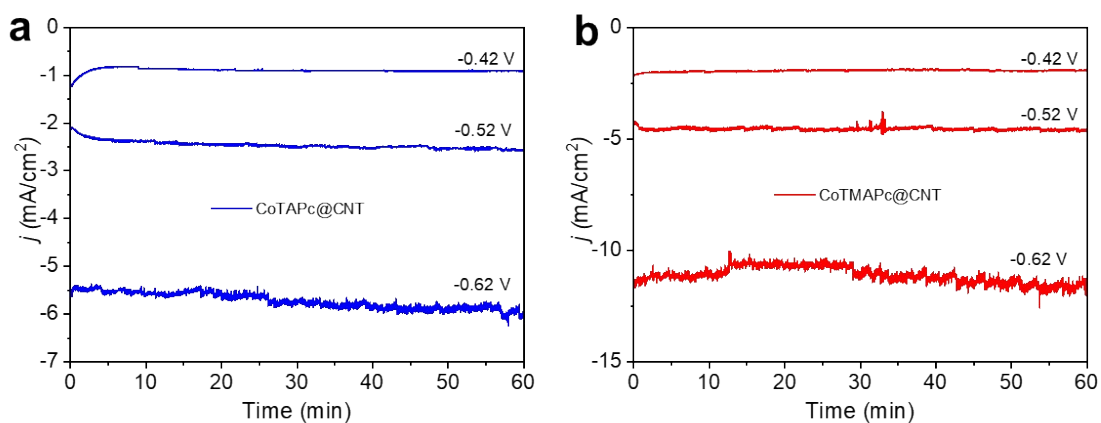


Fig. S13. Chronoamperometric responses of (a) CoTAPc@CNT and (b) CoTMAPc@CNT at different potentials.

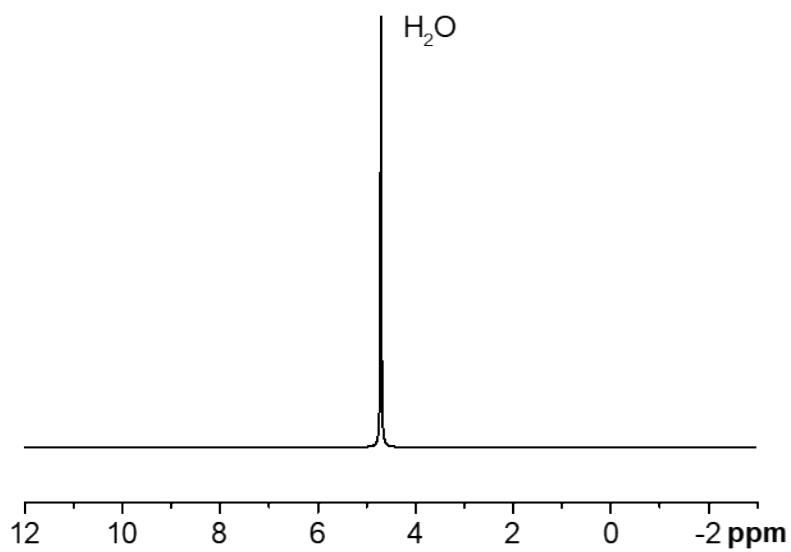


Fig. S14. ¹H NMR spectrum of the liquid products were measured in D₂O and no liquid products were identifiable. The electrolyte was collected from the chronoamperograms test of CoTMAPc@CNT at -0.62 V vs. RHE for 30 min.

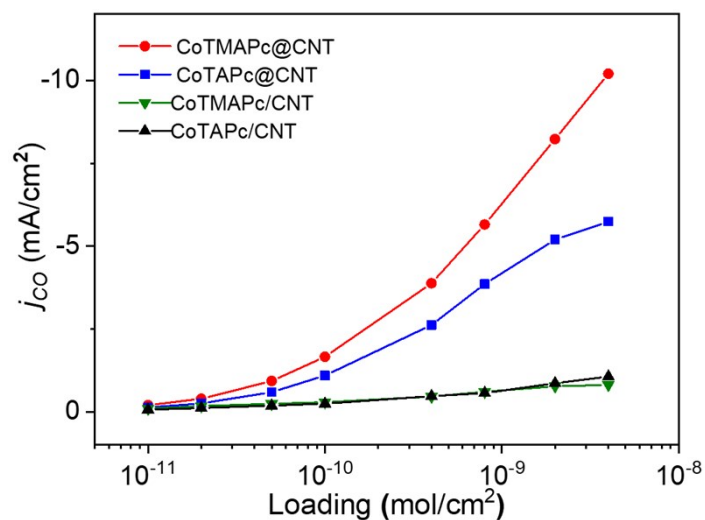


Fig. S15. CO partial current density at -0.62 V vs RHE changing with the catalyst loadings.

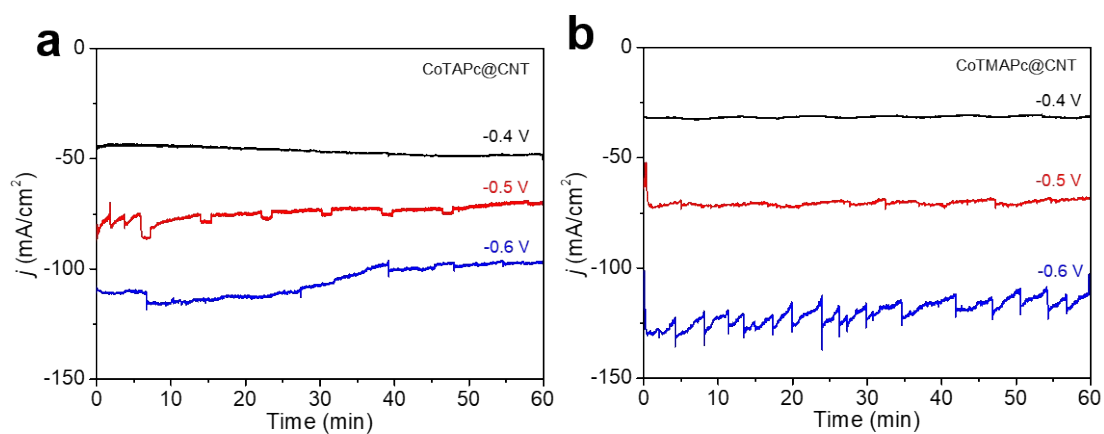


Fig. S16. Current densities of (a) CoTAPc@CNT and (b) CoTMAPc@CNT at various electrolysis potentials in flow cell. For CoTMAPc@CNT, salts segregation on the cathode was observed at -0.6 V, which leads to the fluctuation of current density.

Table S1. The top and side views of CoTAPc and CoTMAPc and their intermediate steps of CO₂RR. The Mulliken charge of Co is highlighted in the table.

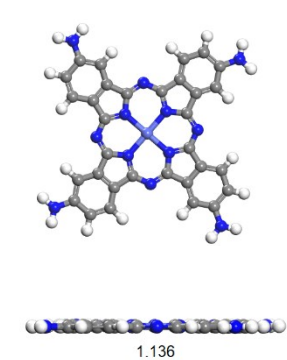
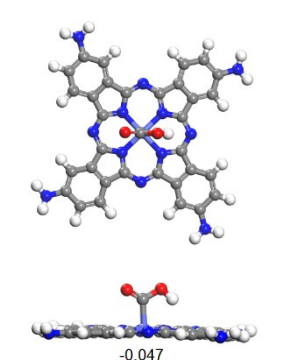
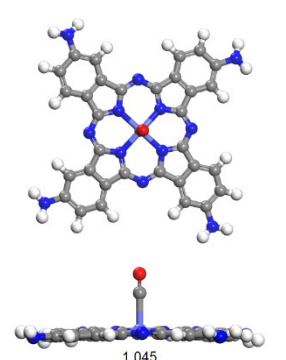
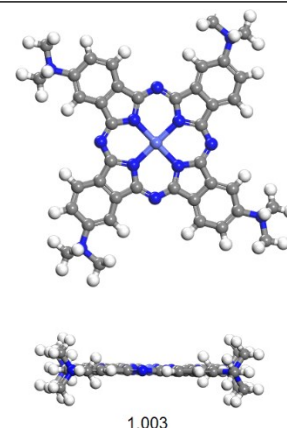
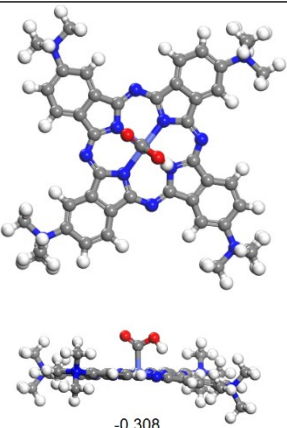
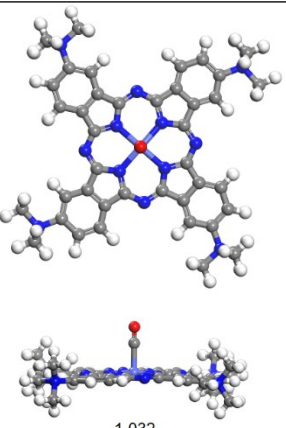
	*	*COOH	*CO
CoTAPc	 1.136	 -0.047	 1.045
CoTMAPc	 1.003	 -0.308	 1.032

Table S2. XPS results analysis for the prepared samples (at. %).

Sample	Element atomic ration (%)				
	C	N	O	Co	N/Co ratio
CoTAPc@CNT	95.36	1.99	2.47	0.18	11.06
CoTMAPc@CNT	95.02	2.31	2.46	0.21	11.00

Table S3. The ICP Co results in the post-reaction electrolyte to quantify the Co leaching.

Samples	ICP Co content (mg/L)	Co leaching percentage (%)
CoTAPc@CNT	0	0
CoTMAPc@CNT	0	0
CoTAPc/CNT	$(1.82 \pm 0.06) \times 10^{-2}$	11.6
CoTMAPc/CNT	$(6.76 \pm 0.05) \times 10^{-2}$	43.0

* The catalyst loading at the electrode was 1 mg/cm².

The electrolyte was collected from the chronoamperograms test of four samples at -0.62 V vs. RHE in CO₂ saturated KHCO₃ for 30 min. The 1 mL electrolyte was extracted from the cell and then nitrated by adding 4 mL concentrated HNO₃ at 90 °C for half an hour. Then the solution was diluted with 15 mL DI water to conduct the ICP analysis. The Co leaching percentage (%) was calculated as following:

$$\text{Co leaching percentage (\%)} = \frac{\frac{6.76 \times 10^{-2} \text{ mg/L}}{1000} \times 20 \times 1.75 \text{ mL}}{1 \text{ mg} \times 0.55\%} = 43 \%$$

Table S4. The CO partial current density (j_{CO}) at different potentials of carbon paper (CP) without deposited catalyst tested in CO₂ saturated 0.5 M KHCO₃ and CoTMAPc@CNT with a molecular loading of 7×10^{-9} mol/cm² tested in N₂ saturated 0.5 M KHCO₃.

Potential (V vs. RHE)	j_{CO} (mA/cm ²)	
	Carbon paper (CO ₂)	CoTMAPc@CNT (N ₂)
-0.57	0	0.084
-0.62	0	0.12
-0.67	0	0.17
-0.72	0.037	0.34

The very small amount of CO production for N₂ fed CoTMAPc@CNT sample is due to the change of HCO₃⁻ to CO₂ from KHCO₃ electrolyte. These relatively small j_{CO} confirm that the negligible CO production without CO₂ or with CO₂ but in the absence of catalyst and CO₂.

Table S5. Comparison of electrochemical performance of CO₂RR catalysts in flow cell.

Catalyst	j (mA/cm ²)	Cell voltage (V)	FE _{CO} (%)	Reference
CoTMPc@CNT	239	-2.3	95.6	This work
CoPc	184	-2.5	95	1
CoPc-CN/CNT	146	-2.3	56	2
Ni-SAC	50	-2.78	97	3
Ni-SAC	130	-2.7	99	4
Au	186	-2.25	85	5
Ag	213	-3	90	6

Method 1: Calculation of the surface active Co site

The electroactive amounts were estimated based on the plot of peak current of the Co^I/Co^{II} oxidation wave (Fig.S11). The amount of electrochemically surface active Co site is calculated according to equation:

$$\Gamma = \frac{Q}{nFA}$$

Where Γ is the electroactive amounts of Co site.

Q is the integration of the anodic peak.

n is the electron number of redox consumed (one-electron process).

F is the Faraday constant (96485 C/mol).

A is the electrode area (1 cm²).

For example, the active site in Figure S11a is calculated as below:

$$\Gamma = \frac{0.663 \times 10^{-3}}{1 \times 96485 \times 1} = 6.87 \times 10^{-9} \text{ mol/cm}^2$$

Method 2: Calculation of faradaic efficiency

$$FE_{gas}(\%) = \frac{Q_{gas}}{Q_{total}} \times 100\% = \frac{\left(\frac{v}{60s/min}\right) \times \left(\frac{V_{gas}}{22400cm^3}\right) \times N \times F \times 100\%}{j}$$

v is gas flow rate controlled by mass flowmeter (10 sccm) at room temperature.

V_{gas} is volume concentration of CO or H₂ in the outlet gas from the cell.

N is the number of electrons required to form a molecule of CO or H₂ (2e⁻).

F is the Faraday constant (96485 C/mol).

j is the recorded current.

Method 3: Calculation of TOF and TON

Turnover frequency (TOF) is defined as the number of reduction product generated per electrocatalytic active site per unit time, calculated as follows:

$$TOF = \frac{j_{tot} \times FE_{co}}{2F \times n_{tot}}$$

n_{tot} is the total loading amount of molecular catalysts determined from the ICP analysis.

Turnover number (TON) is defined as the mole of reduction product generated per electrocatalytic active site over a given period of time, calculated as follows:

$$TON = \frac{Q \times FE_{co(average)}}{2F \times n_{tot}}$$

Q is the total reduction charge amount during the long-term electrocatalysis test. $FE_{co(average)}$ is the average CO faradaic efficiency during the test period.

Method 4: Detailed calculation process:

The density functional theoretical (DFT) calculations were carried out with the Gaussian 16.⁷ The Becke exchange functional (B) and the Lee–Yang–Parr (LYP) correlation functional within a generalized gradient approximation (GGA) was used to describe the interaction between the ionic cores and electrons.⁸⁻⁹ The hybrid basic set was employed to optimize all structures and calculate Gibbs free energy. For H, C, N and O atoms, the basis set b3lyp/6-311+g(d,p) was adopted here. For the metal atom Co, the outer and inner shell valence electrons are described by the effective pseudopotential double- ζ (LANL2DZ) basis set, separately from the core electrons, which were described by the LANL2 effective core potential (ECP). For reaction steps involving transfer of a H^+/e^- pair, the free energy of the pair was set as half the free energy of gaseous H_2 ($H^+ + e^- \leftrightarrow 1/2H_2$).¹⁰

The binding energy (E_b) of an adsorbate was calculated as:

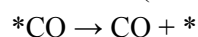
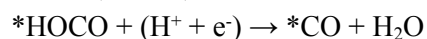
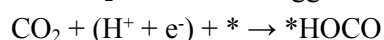
$$E_b = E_{\text{tot}} - E_{\text{molecular}} - E_{\text{adsorbate}}$$

where E_{tot} , $E_{\text{molecular}}$ and $E_{\text{adsorbate}}$ are the total energy of molecular with adsorbate, the energy of clean molecular and the energy of adsorbate in the gas phase, respectively. The change in free energy (ΔG) under room temperature is calculated as

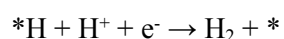
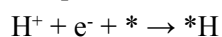
$$\Delta G = \Delta E + \Delta ZPE - T\Delta S$$

where ΔE is the binding energy of adsorbed species, ΔZPE and $T\Delta S$ are the changes of zero-point energy and entropy of a species, respectively.

The CO_2RR to CO is suggested to proceed via the following sequential steps:¹¹



In aqueous electrolytes, the HER inevitably takes place via the following sequential steps,¹² and competes with the CO_2RR :



where * indicates adsorption sites.

References

- 1 S. Ren, D. Joulié, D. Salvatore, K. Torbensen, M. Wang, M. Robert, C. P. Berlinguette, *Science.*, 2019, **365**, 367–369.
- 2 X. Lu, Y. Wu, X. Yuan, L. Huang, Z. Wu, J. Xuan, Y. Wang and H. Wang, *ACS Energy Lett.*, 2018, **3**, 2527–2532.
- 3 K. Jiang, S. Siahrostami, T. Zheng, Y. Hu, S. Hwang, E. Stavitski, Y. Peng, J. Dynes, M. Gangisetty, D. Su, K. Attenkofer and H. Wang, *Energy Environ. Sci.*, 2018, **11**, 893–903.
- 4 T. Zheng, K. Jiang, N. Ta, Y. Hu, J. Zeng, J. Liu and H. Wang, *Joule*, 2019, **3**, 265–278.
- 5 S. Verma, Y. Hamasaki, C. Kim, W. Huang, S. Lu, H. R. M. Jhong, A. A. Gewirth, T. Fujigaya, N. Nakashima and P. J. A. Kenis, *ACS Energy Lett.*, 2018, **3**, 193–198.
- 6 R. B. Kutz, Q. Chen, H. Yang, S. D. Sajjad, Z. Liu and I. R. Masel, *Energy Technol.*, 2017, **5**, 929–936.
- 7 Gaussian 16, Revision A.03, M. J. Frisch, G. W. Trucks, H. B. Schlegel, G. E. Scuseria, M. A. Robb, J. R. Cheeseman, G. Scalmani, V. Barone, G. A. Petersson, H. Nakatsuji, X. Li, M. Caricato, A. V. Marenich, J. Bloino, B. G. Janesko, R. Gomperts, B. Mennucci, H. P. Hratchian, J. V. Ortiz, A. F. Izmaylov, J. L. Sonnenberg, D. Williams-Young, F. Ding, F. Lipparini, F. Egidi, J. Goings, B. Peng, A. Petrone, T. Henderson, D. Ranasinghe, V. G. Zakrzewski, J. Gao, N. Rega, G. Zheng, W. Liang, M. Hada, M. Ehara, K. Toyota, R. Fukuda, J. Hasegawa, M. Ishida, T. Nakajima, Y. Honda, O. Kitao, H. Nakai, T. Vreven, K. Throssell, J. A. Montgomery, Jr., J. E. Peralta, F. Ogliaro, M. J. Bearpark, J. J. Heyd, E. N. Brothers, K. N. Kudin, V. N. Staroverov, T. A. Keith, R. Kobayashi, J. Normand, K. Raghavachari, A. P. Rendell, J. C. Burant, S. S. Iyengar, J. Tomasi, M. Cossi, J. M. Millam, M. Klene, C. Adamo, R. Cammi, J. W. Ochterski, R. L. Martin, K. Morokuma, O. Farkas, J. B. Foresman, and D. J. Fox, Gaussian, Inc., Wallingford CT, 2016.
- 8 B. Delley, *J. Chem. Phys.*, 2000, **113**, 7756–7764
- 9 B. Delley, *J. Chem. Phys.*, 1990, **92**, 508–517
- 10 Peterson, A. A.; Abild-Pedersen, F.; Studt, F.; Rossmeisl, J.; Nørskov, J. K. How Copper Catalyzes the Electroreduction of Carbon Dioxide into Hydrocarbon Fuels. *Energy Environ. Sci.* 2010, **3**, 1311–1315
- 11 W. L. Zhu, R. Michalsky, O. Metin, H. F. Lv, S. J. Guo, C. J. Wright, X. L. Sun, A. A. Peterson and S. H. Sun, *J. Am. Chem. Soc.*, 2013, **135**, 16833–16836
- 12 K. J. Vetter, *Electrochemical Kinetics: Theoretical and Experimental Aspects*, Academic Press, New York, 1967.